

## Article

# Research on Mechanical Behavior and Energy Evolution of Coal and Rocks with Different Thin Spray-On Liners Thickness under Uniaxial Compressive Loading

Yixin Zhao <sup>1,2,\*</sup>, Xiang Fu <sup>1,2,3</sup>, Yangyang Shi <sup>1,2</sup>, Bowen Zhao <sup>1,2</sup>, Xingyu Fu <sup>1,2,4</sup>, Xiufeng Zhang <sup>5</sup> and Yang Chen <sup>5</sup>

<sup>1</sup> Beijing Key Laboratory for Precise Mining of Intergrown Energy and Resources, China University of Mining & Technology-Beijing, Beijing 100083, China; soarfox2002@126.com (X.F.); s1996yy@163.com (Y.S.); mrzhaojere@163.com (B.Z.); fxy10026@163.com (X.F.)

<sup>2</sup> School of Energy and Mining Engineering, China University of Mining & Technology-Beijing, Beijing 100083, China

<sup>3</sup> Beijing Research Institute of Coal Chemistry, China Coal Research Institute, Beijing 100013, China

<sup>4</sup> China Coal Research Institute, Beijing 100013, China

<sup>5</sup> Shandong Energy Group Co., Ltd., Jinan 250014, China; 13953863379@163.com (X.Z.); chenyang-812006@163.com (Y.C.)

\* Correspondence: zhaoyx@cumtb.edu.cn

**Abstract:** Compared with the traditional supporting materials such as the bolts, mesh, and concrete, thin spray-on liners (TSLs) have the advantages of improving impact energy bearing and absorption capacity of rocks. In this study, the uniaxial compressive mechanical response feature of white sandstone, yellow sandstone, and coal with different coating thickness of TSLs were investigated through laboratory tests and theoretical analysis. The hard segments and soft segments of TSLs induced microphase separation, and formed the physical cross-linking. The hard segment evenly dispersed in the soft segment, which improved the mechanical strength of the TSLs. The confining pressure was affected by the TSL-coated coal and rocks, which improved the mechanical strength of the rocks and coal under UCS loading. It was discovered that the uniaxial compressive strength (UCS) increases with an increase in the TSL coating thickness, and UCS increments of the coated white sandstone, yellow sandstone and coal were 4.6%, 25.51%, and 43.75%, respectively. The energy absorption capacities of the coated coal, and yellow and white sandstones gradually decreased with an increase in their TSLs coating thickness. Meanwhile, the energy-absorbing capacity of a coated rock reduced gradually as rock coating decreases. Furthermore, the energy-absorbing capacity of coal is greater than that of yellow sandstone or white sandstone. By increasing the coating thickness, the total and dissipative energies in the yellow sandstone, white sandstone, and coal specimens were gradually increased, and energy increment was significantly more in coal (2–3 times), while the elastic energy remained nearly unchanged.

**Keywords:** coal and rock; uniaxial compression; TSLs; stress-strain curve; energy-absorbing



**Citation:** Zhao, Y.; Fu, X.; Shi, Y.; Zhao, B.; Fu, X.; Zhang, X.; Chen, Y. Research on Mechanical Behavior and Energy Evolution of Coal and Rocks with Different Thin Spray-On Liners Thickness under Uniaxial Compressive Loading. *Sustainability* **2022**, *14*, 5909. <https://doi.org/10.3390/su14105909>

Academic Editor: Adam Smoliński

Received: 4 April 2022

Accepted: 6 May 2022

Published: 13 May 2022

**Publisher's Note:** MDPI stays neutral with regard to jurisdictional claims in published maps and institutional affiliations.



**Copyright:** © 2022 by the authors. Licensee MDPI, Basel, Switzerland. This article is an open access article distributed under the terms and conditions of the Creative Commons Attribution (CC BY) license (<https://creativecommons.org/licenses/by/4.0/>).

## 1. Introduction

With the development of deep excavation technologies for coal mine, problems such as high ground stress, high hydraulic pressure, high ground temperature and engineering excavation disturbance have emerged. These stresses destabilize coal strata, and cause frequent deep excavation disasters, especially rock burst [1] which refers to non-linear deformation of rocks caused by the elastic strain energy accumulated in them owing to severe excavation.

The rock burst mechanism has been researched by several universities and institutes [2]. It has caused geologic hazards and operation worker injuries and equipment unsafe. A rock burst accident scene accident diagram as shown in Figure 1. As an example of 12# mine of Pingdingshan Coal Group, rock burst prevention requires timely roadway and

ground support after excavation, and changes in rock stress condition must be considered. Some traditional techniques including using rock bolts, shotcrete, and wire mesh, or a combination of these.



**Figure 1.** Diagram of rock burst scene accident.

Rock bolt support techniques have been researched in China since 1956, and now they are a primary positive support technique used in mine excavation [3]. Rock bolts have a dominating effect, and initial stress and its dissipation play a decisive role in rocks support [4]; however, they have some limitations. Wire mesh can prevent small rocks from falling, and it diffuses the initial stress to the surrounding rocks by combing with plate and metal band, which is important to control loosening and deformation of surrounding rocks in the initial stage [5]. However, the yielding capacity support of wire mesh is effective when the surrounding rocks contain several deformations. Shotcrete seals the rock skin, thereby preventing rock weathering and slake reduction by bonding the joints and fractures. It is a brittle material that cannot withstand the rock tensile stress and can be destroyed easily; hence, it cannot stably support the rock and strata. Moreover, the thickness of shotcrete is more than 50 mm, which can be hazardous when it breaks and falls. Furthermore, its application has several problems such as low operation speed, increased dust, increased labor, high elasticity, and high logistic. Therefore, a new surface rock support technology with higher strength properties, rapid curing time and an improved yielding capacity is required to significantly improve rock stability.

A thin spray-on Liner (TSL) is a chemical membrane with a thickness of approximately 2–5 mm, which is sprayed onto the rock surfaces to support the rock mass [6]. TSLs comprise organic materials such as polyurethane, polyurea, acrylate, methacrylate and cementitious polymer. TSLs offer various advantages such as high adhesion properties, high tensile strength, prevention of air ingress in rocks and the ability to penetrate open joints and fractures of rock to be TSLs-rock composites [7–11]. They stick to the key loosen blocks of a rock mass and help interlock a fractured rock, and minimize the disintegration of loose rock. The support mechanism of TSLs presented in Figure 2.

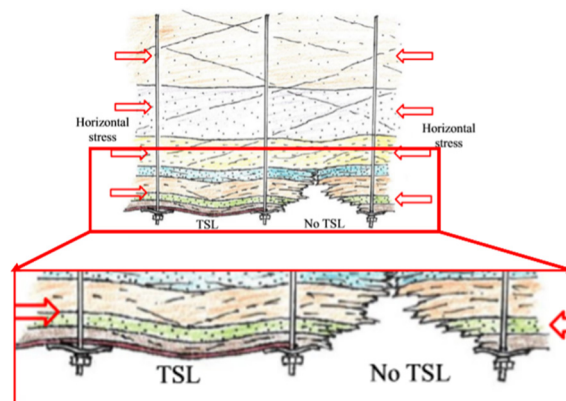


**Figure 2.** Support mechanism of TSL combined with rock matrix [12].

Stacey and Lau's study showed the mechanism of TSLs based on loading behavior and surface support behavior [13]. The support mechanism of a TSL are as follows [14–18]: (1) Basket mechanism [8,14,19]: The flexural and tensile strengths of a TSLs bearing the rock gravity load when it works as an independent support structure. It forms a bearing basket to support the loosened rocks or unstable key blocks. (2) Glue mechanism [15,17,20–22]: sprayed TSLs can penetrate the joints and fractures of a rock, adhere small rocks together as a whole like glue, and promote block interlock. (3) Wedge mechanism [14,18,23,24]: sprayed TSLs penetrate the joints and fractures and grout the dilatation space of crevices, such that friction force between rocks and strata restricts the rock from falling; hence, TSLs act as a wedge to improve the stability of rocks. (4) Membrane effect [15,16,25–29]: TSLs offer both the shotcrete and bolt mesh effects, and they can function as a sealing skin to prevent irregular gas emissions and water seeping from the ribs and can prevent further weathering. They rehabilitate highly stressed strata to stabilize the loosen rocks.

Although the uniaxial compression test conditions for the combination of TSLs and coal or rock have matured, there are few studies on the mechanical properties and energy evolution process of this combination. To address these issues, this study used professional equipment to control the slurry mixing ratio with high precision and an automatic spray gun to uniformly coat the specimen. The uniaxial compression experiment was performed on various combinations of TSLs and coal or rock, and the evolution law of elastic and dissipation energy during the failure of the coated rock specimen was analyzed. This study demonstrates the improvement of compressive properties of coal and rocks through TSLs coating, and to provides an experimental basis for the application of TSLs in the relevant support fields.

## 2. Mechanical Analysis of TSLs

### 2.1. Preparation and Tensile Testing of the TSLs

Generally, TSLs preparation involves mixing two materials. In this study, one was a pale-yellow sticky liquid, which was marked as A, and the other was a pale gray viscous liquid, marked as B. If A reacts smoothly with B, their viscosity is similar. The viscosities of A and B were 1479 mPa·s and 1493 mPa·s, respectively, which were measured using the NDJ-5S rotary viscometer (Shenzhen Dingxinyi Experimental Equipment Co., Ltd., Shenzhen, China).

A and B were blended and impinged in the reaction chamber at high temperature between 60–80 °C and pressure of approximately 10 MPa, and then sprayed into an elastic membrane. At this time, the TSL was bubbling and had a weak strength owing to a significant pressure difference.

To obtain the mechanical properties of the TSLs, it is necessary to perform tensile mechanical tests on them. A TSL sample was prepared by spraying materials A and B with a sprayer, as shown in Figure 3. The sample was stored in a container that could maintain a constant temperature and humidity, and then cut into a dumbbell shape with an electrohydraulic punching machine. Thereafter, its tensile strength was tested.

To determine the tensile properties of TSLs, ASTM D638 Type-IV dumbbell test specimens were molded and tested [30]. The dumbbell shape is shown in Figure 3; the thickness of the TSLs sprayed on the acrylate plate was approximately 3 mm, and the sample was leveled with a spatula to maintain a uniform thickness. To cure dry, and solidify the sample, it was stored in a container that maintain a constant temperature (25 °C and humidity (50%) for seven days.

After removing the sample from the container, it was cut with a CP-1 electrohydraulic punching machine in a dumbbell shaped mold. The scraper modified the sample surface to maintain a smooth outline. The constant load rate was 10 mm/min until the failure occurred.

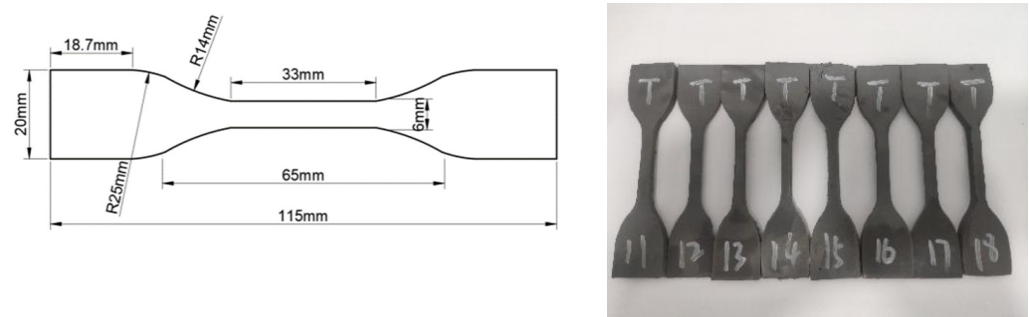


Figure 3. Type IV Dumbbell specimen [30].

The tensile loading of the sample induced the highest stresses in the narrow sections of the center parts. The specimen must self-align with the direction of the pull to prevent inaccurate results owing to eccentric loading. The tensile strength was tested under the displacement control mode, and the loading and displacement were recorded through the testing process. The result was only considered valid when the dumbbell specimen broke at the narrow section, Figure 4 shows the results of this experiment, wherein five specimens are valid damaged, and the breaking site of sample number 18 is not in the middle; hence, the breakage is invalid.



Figure 4. Damage diagram of type IV dumbbell specimen.

The tensile strength of TSLs, averaged tensile strength, elongation, and shore hardness of the TSLs are listed in Table 1.

Table 1. Test results of type IV dumbbell sample.

Specimen Number	Curing Time/d	Tensile Strength/MPa	Average Tensile Strength/MPa	Elongation/%	Shore A	Shore D
IV-TSL12	7	23.79	24.44	526.49	91.5	45.5
IV-TSL13	7	25.53		434.71	91	46
IV-TSL14	7	23.63		313.89	92	45
IV-TSL15	7	21.84		228.19	91.5	45
IV-TSL16	7	27.41		401.09	92	45.5
IV-TSL18	7	NA		NA	NA	NA

## 2.2. SEM Analysis of the TSLs

According to the information presented in Table 1, the tensile strength of IV-TSL 16 is maximal and that of IV-TSL 18 is zero. The scanning electron micrograph of the fracture surface after curing both IV-TSL16 and IV-TSL 18 for seven days is shown in Figure 5. The hard segment and soft segments of TSLs cause microphase separation and form physical cross-links when material A reacts with B. Previously, the hard segment was dispersed

evenly in the soft segment to improve the mechanical strength of the TSLs [31,32]. IV-TSL 16 was sprayed such that material A and B reacted completely; hence, the TSLs were stable. IV-TSL 18 exhibits a bump in the SEM, which prohibited an effective microphase separation, and its tensile strength was weak; therefore, it broke easily when tensile strength was applied to it.

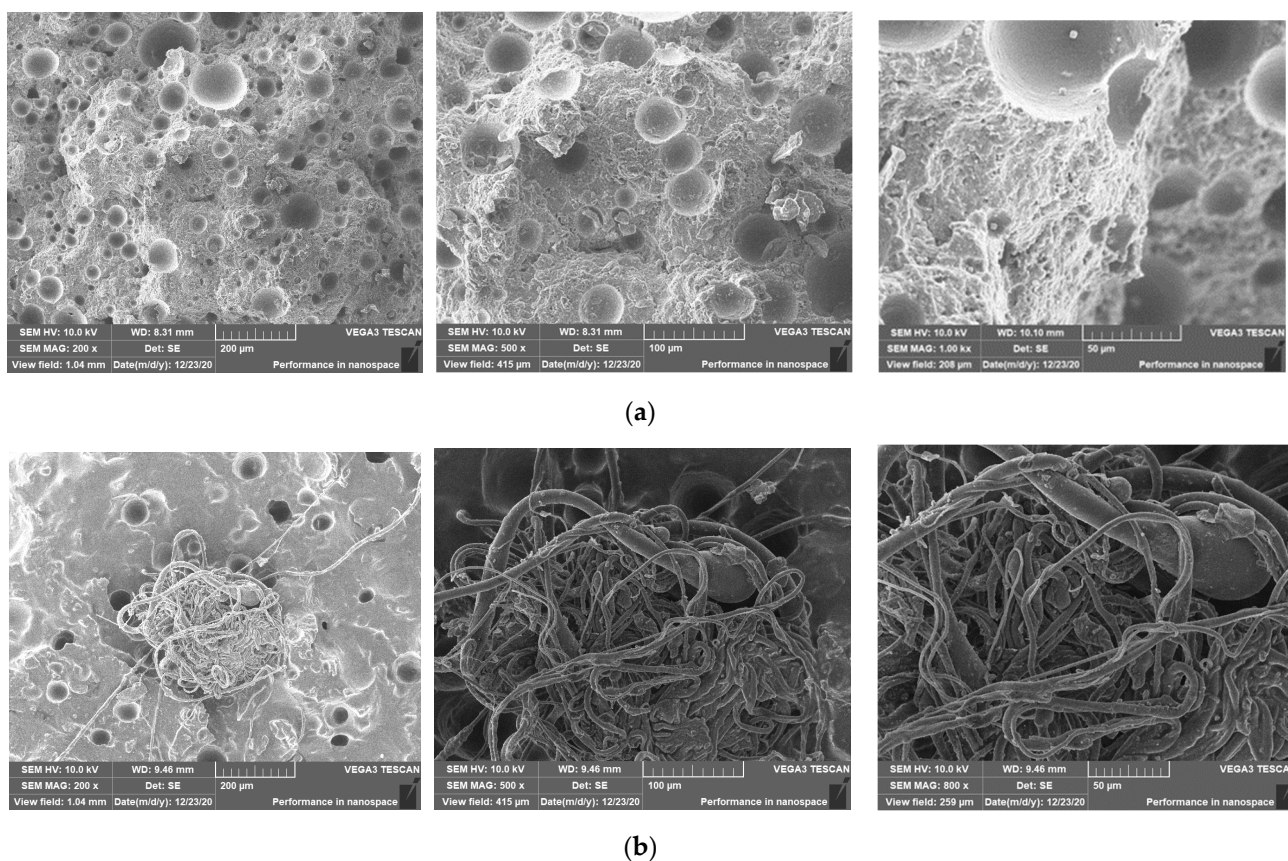


**Figure 5.** SEM image of the fracture of IV-TSL specimens: (a) IV-TSL16 specimen, (b) IV-TSL18 specimen.

### 3. Compression Test of the Combination of TSLs and Coal and Rock

#### 3.1. Preparation of the Combination of TSLs and Coal-Rock

Preparation of the specimen: 18 samples of yellow sandstone and 15 samples of white sandstone were obtained from Sichuan Zigong, and 15 of coal were obtained from Zhaoguo coal mine in Jiaozuo, Henan Province. These specimens were configured in cylindrical shape ( $D = 50$  mm,  $H = 100$  mm), and then used in UCS test.

The reaction of material A and B was performed in a Graco E-10 hp mini chamber. The specimens were then sprayed with different coating thicknesses of the obtained TSL, which were 2 mm, 3 mm, 4 mm, and 5 mm. Uncoated specimen and those coated with the TSL are shown in Figure 6. The specimen surface was leveled with a scraper to maintain a uniform thickness. The coated and uncoated specimens were solidified in a constant temperature ( $25$  °C) and humidity (50%) curing box for seven days. The UCS experiments were conducted on MTS E45.305, and the loading velocity was 0.1 mm/min. The rock mass deformation destruction characteristics, acoustic emission spatial-temporal evolution pattern and micro destruction mechanism of coated and uncoated specimens were analyzed.

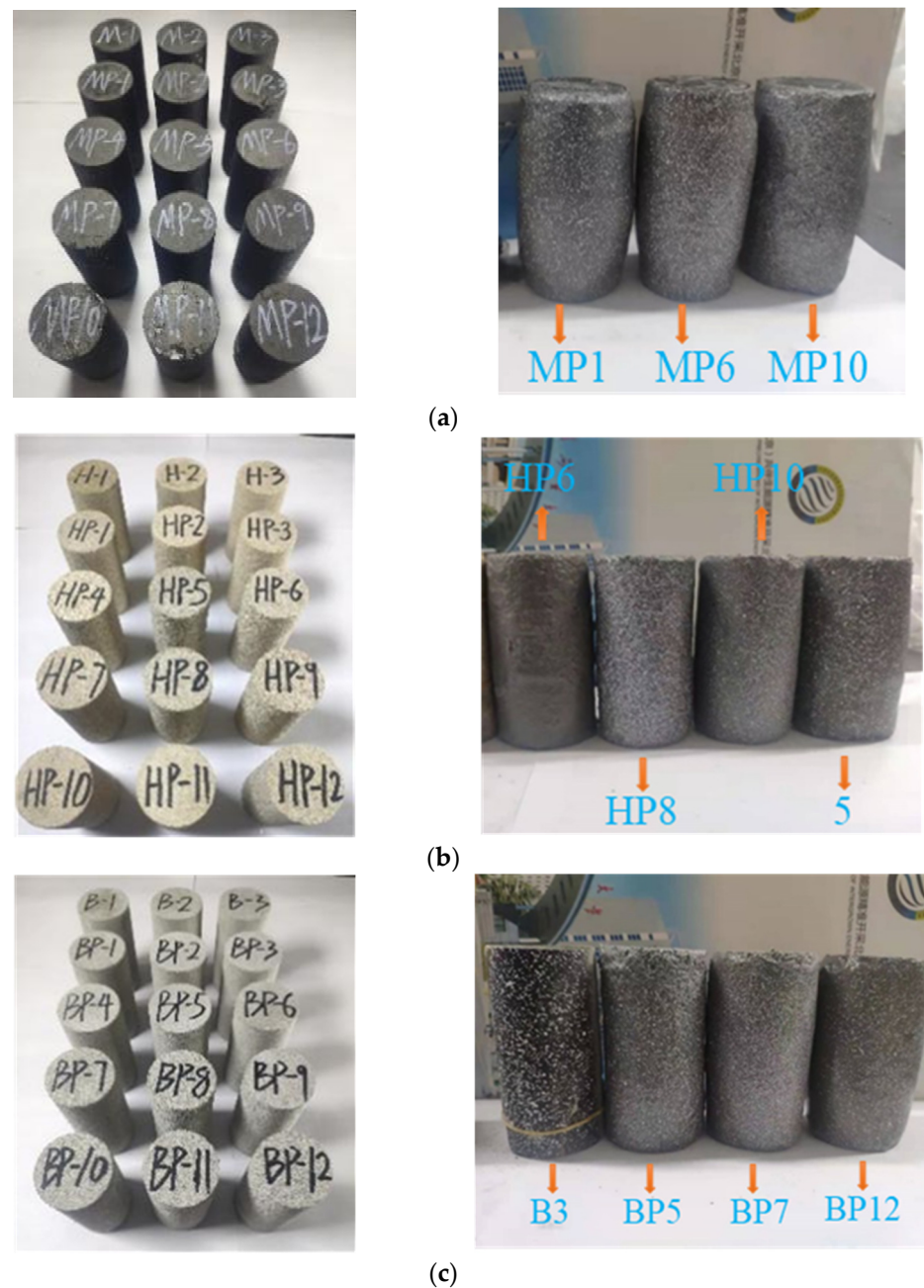


**Figure 6.** Different TSL uncoated and coated rock materials: (a) Coal specimens, (b) Yellow sandstone specimens, (c) White sandstone specimens.

### 3.2. Primary Parameter Analysis

The average density of Zhaogu coal, white and yellow sandstones, respectively,  $1.467 \text{ g/cm}^3$ ,  $2.440 \text{ g/cm}^3$ , and  $2.322 \text{ g/cm}^3$ , its volatility range of  $1.446\text{--}1.490 \text{ g/cm}^3$ ,  $2.418\text{--}2.455 \text{ g/cm}^3$ ,  $2.276\text{--}2.362 \text{ g/cm}^3$ , respectively. As shown in Table 2.

The primary wave (P-wave) indicated an astonishing property of the coal interior. Because the UCS has a positive correlation with the P-wave velocity under the uniaxial loading, P-wave was used to identify mechanical characteristics and estimate rock mechanism parameters [33–35].

**Table 2.** Physical parameters of coal and rock without spraying and with different spraying thicknesses.

	Thickness TSL Coated mm	No.	M/g	Velocity m/s	Elastic Modulus GPa	Uniaxial Compressive Strength MPa	Density g/cm <sup>3</sup>
Coal	0	M2	275.5	1847.22	2.476	15.89	1.467
	0	M3	274.0	1344.86	2.647	17.62	1.446
	0	19	279.0	1837.61	2.356	13.80	1.467
	2	MP1	276.0	1892.34	2.411	19.28	1.467
	2	MP2	287.0	1742.40	NA	NA	1.470
	2	MP3	271.0	1929.65	1.743	23.15	1.456
	3	MP4	275.0	1821.82	2.715	22.03	1.462
	3	MP5	287.0	1728.45	NA	NA	1.468
	3	MP6	276.5	1869.53	2.696	23.31	1.484
	4	MP8	279.5	1668.48	NA	NA	1.490
	4	MP10	269.5	1920.42	2.003	22.34	1.456
	4	MP11	279.0	1804.20	2.521	20.16	1.466
White Sandstone	0	B1	469.3	2339.52	NA	NA	2.433
	0	B3	471.0	2267.32	4.546	41.51	2.434
	0	38	471.0	2180.94	4.388	42.30	2.440
	2	BP4	467.9	2187.54	NA	NA	2.436
	2	BP5	466.0	2184.88	3.811	38.42	2.430
	2	BP6	469.3	2253.59	3.763	37.92	2.418
	3	BP7	467.9	2200.44	4.252	42.99	2.426
	3	BP8	471.4	2275.45	3.879	40.98	2.452
	3	BP9	472.1	2227.99	3.570	45.18	2.453
	4	BP10	472.2	2185.14	4.198	42.36	2.446
	4	BP11	470.2	2258.71	NA	NA	2.455
	4	BP12	472.1	2241.89	4.294	45.30	2.438
Yellow Sandstone	0	H1	428.3	1793.17	3.448	38.28	2.289
	0	H2	428.2	1728.80	3.344	34.94	2.290
	0	H3	441.7	1702.78	NA	NA	2.278
	2	HP-4	427.5	1741.35	3.357	35.24	2.276
	2	HP-5	448.0	1639.02	NA	NA	2.362
	2	HP-6	429.5	1717.28	3.481	37.45	2.287
	3	HP7	439.3	1717.79	NA	NA	2.344
	3	HP8	449.4	1717.24	3.872	40.98	2.357
	3	HP-9	440.0	1868.12	4.016	39.61	2.350
	4	HP10	451.1	1718.00	4.197	42.36	2.361
	4	HP-11	429.5	1725.17	NA	NA	2.287
	4	HP12	430.5	1784.26	3.432	41.46	2.292
	5	5	440.5	1900.44	3.762	46.40	2.371
5	7	442.5	2244.93	4.384	45.50	2.351	
5	20	444.0	2107.28	NA	NA	2.358	

After being curing for seven days, the specimens were tested under ultrasonic velocity. Yellow sandstone (HP), white sandstone (BP), and coal (MP) were classified into groups based on their coating thickness: 0 mm, 2 mm, 3 mm, 4 mm, and 5 mm. Each group contained three samples. As listed in Table 2, the average velocities of white sandstone, yellow sandstone, and coal were 2238.92 m/s, 1790.80 m/s and 1783.91 m/s, respectively. The P-wave velocity gradually increased with the density improvement of the specimen. It was maximal for the white sandstone and minimum for coal because the bigger grain clearance and porosity, the smaller the density of the specimen; therefore the ultrasonic attenuation was significant during its propagation.

From Table 2, it is evident that the elastic modulus and uniaxial compressive strength of white and yellow sandstone are significantly higher than that of coal. This could be because the sandstones are more compact than coal.

### 3.3. Loading System

MTS E45.305 loading system, the axial loading about 0–300 kN, loading velocity is 0.005–500 mm/min, which can record data and plot stress-strain curve in Figure 7.

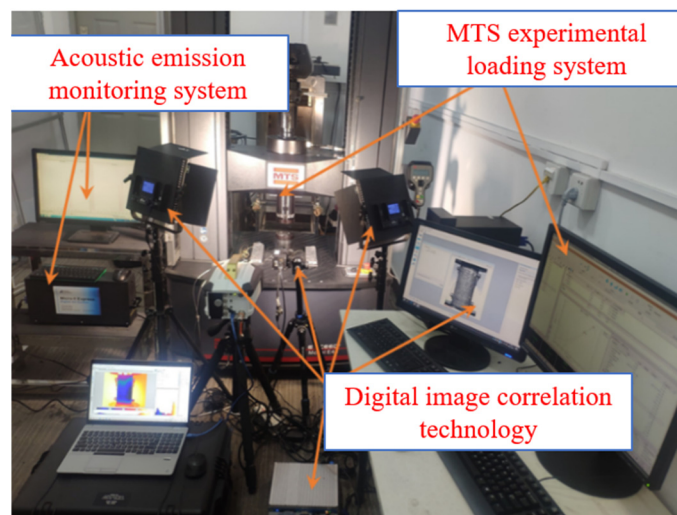


**Figure 7.** Uniaxial compression test detection system.

## 4. Compression Test Results and Analysis

### 4.1. Analysis of Compressive Mechanical Properties of Specimens

#### 1. Mechanical behavior of coal specimen coated with TSL.

Figure 8 shows a comparison of the stress-strain curves of the uncoated coal and those coated with 2 mm, 3 mm and 4 mm of TSL. Each group of 2 mm, 3 mm and 4 mm TSL coated coal had one specimen that broke due to wrong operation; therefore, these specimens' curve were not included in the Figure 8. Compared with the uncoated coal, the UCS gradually increased with the coated thickness in the coated coal. It is evident that the stress-strain curve changes with the coating thickness and the shape of the uniaxial compressive stress-strain curve of the uncoated coal were sharper than those of coated specimen [36,37]. However, the curve shape of the coated coal was relatively round and gentle, the stress increased and decreased several times with the strain, and there was a step-like stress decreasing trend in the post-peak stage. The maximum peak stress (15.77 MPa) on the stress-strain curve of the uncoated coal was less than that on the coated coal (21.22 MPa (2 mm), 22.67 MPa (3 mm), 21.25 MPa (4 mm)). Thus, the stress gradually increased with the thickness of the TSL coating.

TSLs reinforce coal by imparting a confining pressure-like effect to limit its lateral deformation. Sprayed TSLs penetrate the cracks of the coal and provide considerable adhesive strength, which offers the potential support to its structure. Similar to the confining pressure load rendered by TSLs, the properties of the coal itself are also affected to a certain extent. The primary fractures inside the coal specimen are compacted by the confining pressure before the axial compression is applied. The higher the confining pressure, the better the fracture closure.

As evident from the curve of stress-strain shown in Figure 8, the TSL coating increased both the peak pressure and the residual strength of the coal specimens. Compared with uncoated coal, the peak pressure of coal coated with 2 mm, 3 mm and 4 mm of TSL improved by 34.56%, 43.75% and 34.75%, respectively. The post-peak pressure curve of TSL coated coals was more gradual than that of the uncoated coal, and a step-like pattern was observed on it, which indicates that the TSLs significantly improved the residual strength of the coal, and the confining pressure effect exerted by them reinforced the specimens.

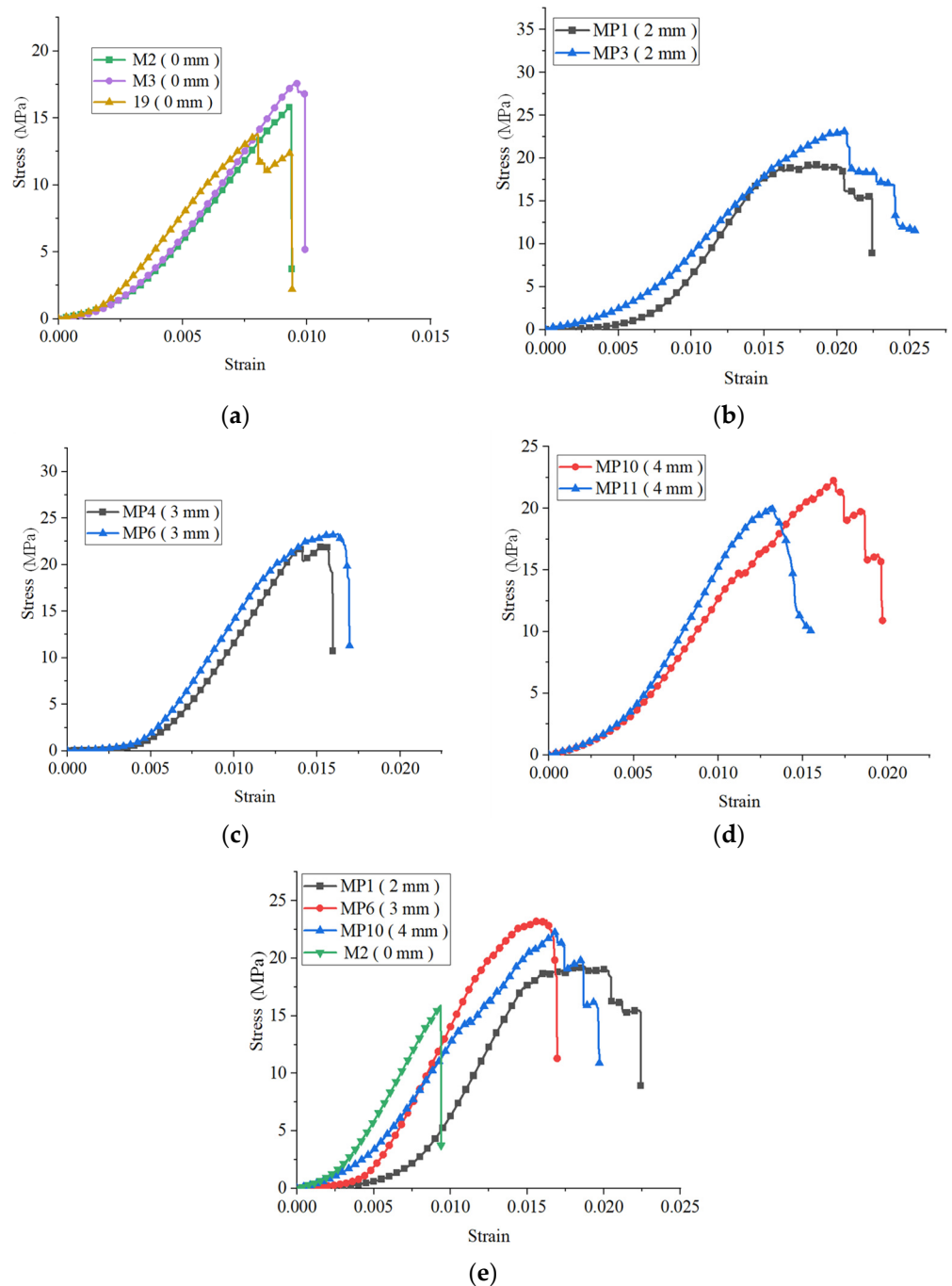


**Figure 8.** Comparison of stress and strain curves of coal with different spray thickness: (a) TSL uncoated coal, (b) 2 mm TSL coated coal, (c) 3 mm TSL coated coal, (d) 4 mm TSL coated coal, (e) TSL coated coal with different thickness.

## 2. Mechanical behavior of yellow sandstone specimen coated with TSL.

Figure 9 shows a comparison of the stress-strain curves of the uncoated yellow sandstone and those coated with 2 mm, 3 mm, and 4 mm of TSL. Similar to the results of the coal specimens, the UCS of the yellow sandstone specimen increased gradually with an increase in the coating thickness. In Figure 9, the uniaxial compressive stress-strain curve of the uncoated yellow sandstone was sharp, and the stress increased and decreased only once with the strain, whereas the curve of the coated ones was relatively round and gentle, and the stress increased and decreased several times with the strain. The peak stress (36.61 MPa) in the stress-strain curve of the uncoated yellow sandstone was less than that of the coated

yellow sandstone (36.65 MPa (2 mm), 40.30 MPa (3 mm), 41.91 MPa (4 mm)). Thus, the stress gradually increased with the thickness of the TSL coating.

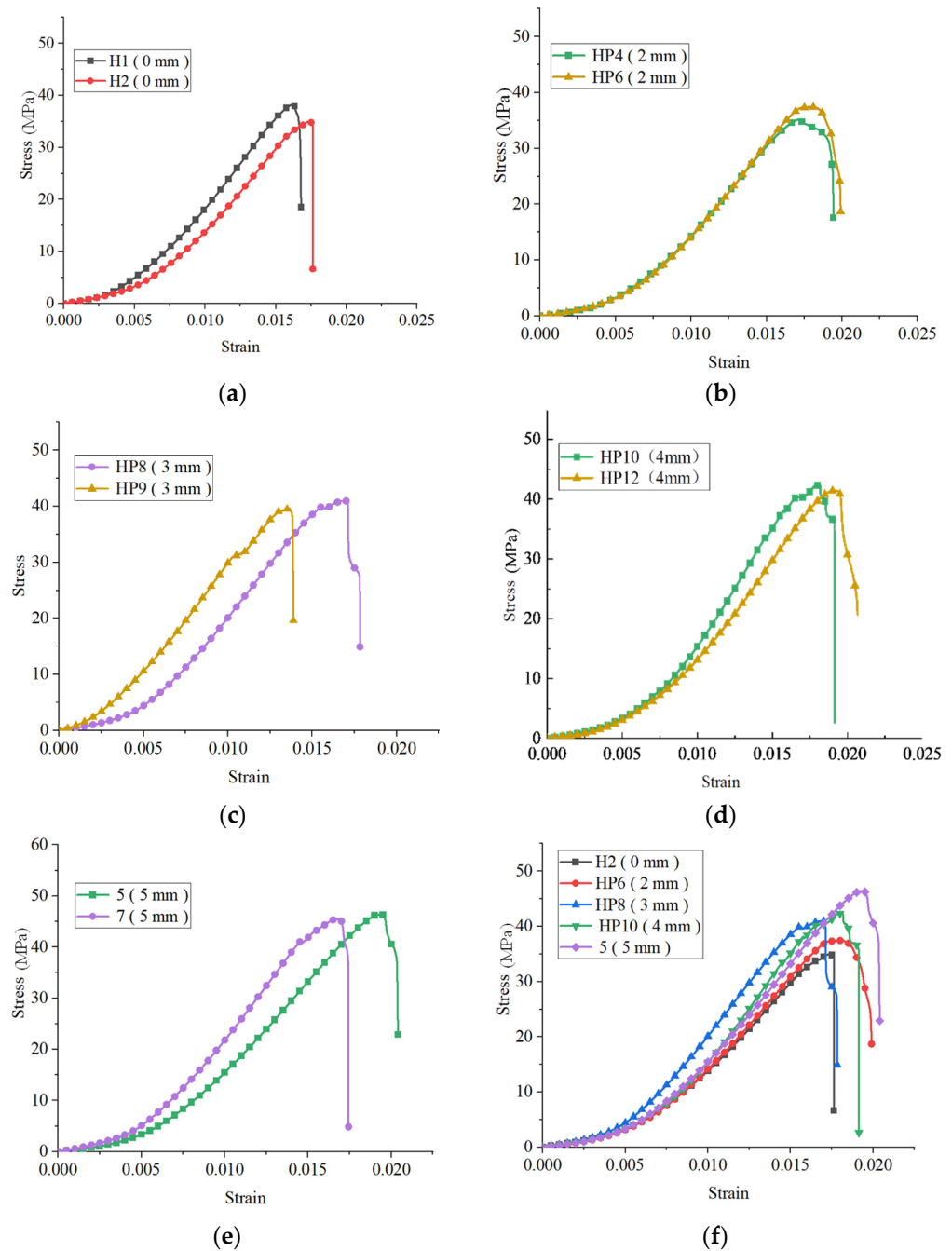


**Figure 9.** Stress-strain curves of yellow sandstone with different spray thickness: (a) TSL uncoated yellow sandstone, (b) 2 mm TSL coated yellow sandstone, (c) 3 mm TSL coated yellow sandstone, (d) 4 mm TSL coated yellow sandstone, (e) 5 mm TSL coated yellow sandstone, (f) TSL coated yellow sandstone with different thickness.

### 3. Mechanical behavior of white sandstone specimen coated with TSL.

Figure 10 shows a comparison of the stress-strain curves of the uncoated white sandstone and those with 2 mm, 3 mm, and 4 mm of TSL coating. Similar to the results of the coal specimens, the UCS of the white sandstone specimen increased gradually with the increasing in the coating thickness. The uniaxial compressive stress-strain curve of the uncoated white sandstone was sharp, whereas the curve of the coated white sandstone was

relatively round and gentle, the stress increased and decreased several times with the strain, and a step-like stress decreasing trend in the post-peak stage was observed. The peak stress (41.9 MPa) in the stress-strain curve of the uncoated white sandstone was smaller than that of the coated white sandstones (38.17 MPa (2 mm), 43.05 MPa (3 mm), 43.83 MPa (4 mm)). Hence, the stress gradually increased with the TSL coating thickness.

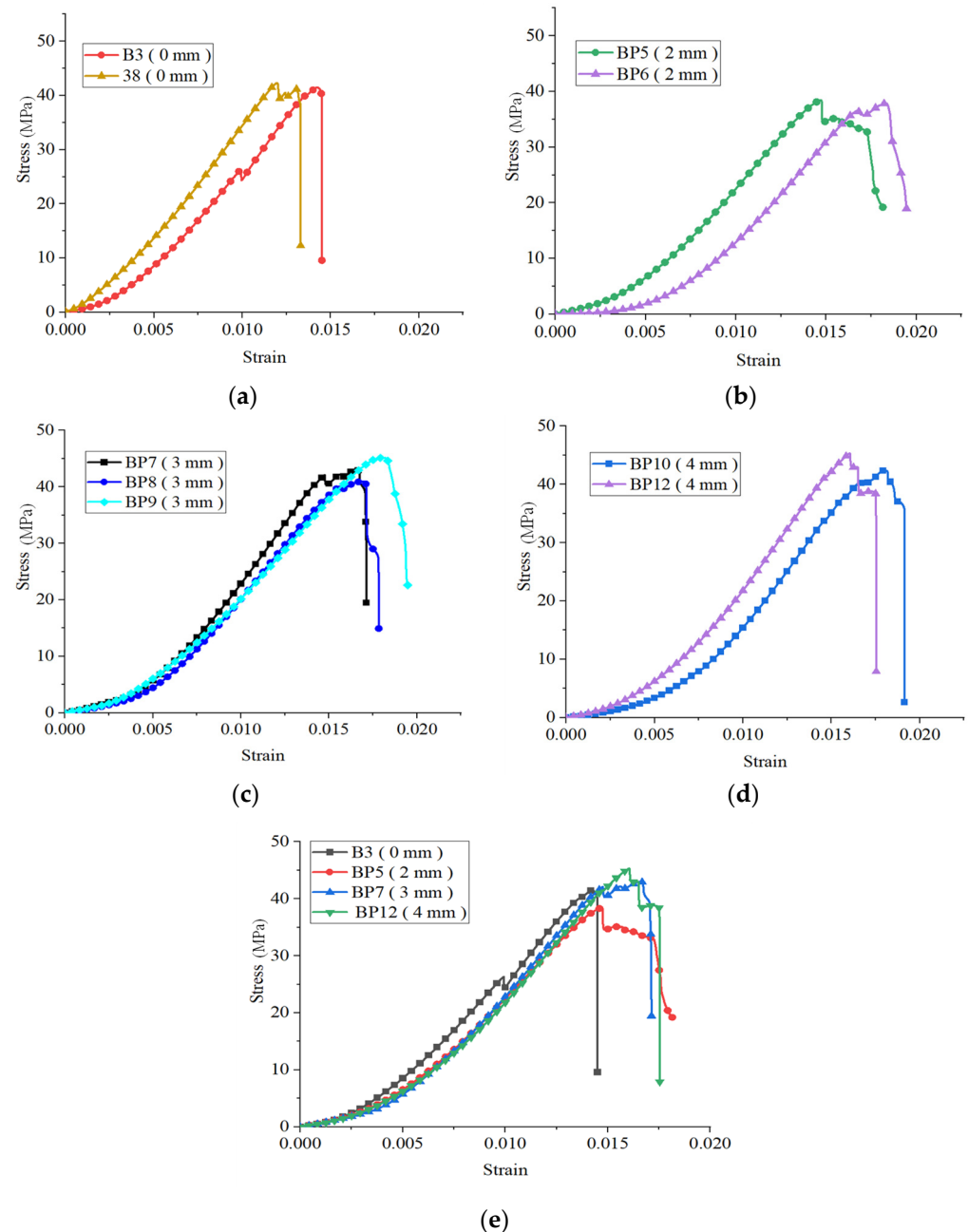


**Figure 10.** Comparison of stress and strain curves of white sandstone with different spray thickness: (a) TSL uncoated white sandstone, (b) 2 mm TSL coated white sandstone, (c) 3 mm TSL coated white sandstone, (d) 4 mm TSL coated white sandstone, (e) TSL coated white sandstone with different thickness.

According to the above Figures, the stress of the TSL-coated yellow and white sandstones improved significantly and increased with the TSL-coating thickness. The stress of coated coal also improved slightly, the suitable coating thickness was 2–3 mm.

#### 4.2. Specimen Energy Evolution Analysis

##### 1. Energy evolution analysis method

During the UCS experiment, the evolution of machine energy can be expressed by five different energies: Elastic energy is stored in the rock interior and escapes when the rock is deformed, it is the main source of energy disaster in rocks. Plastic energy occurs owing to the misalignment of the original crack and the yield of a secondary crack. Surface energy is the energy required for crack propagation when the fracture extends; hence, the plastic and surface energies are dissipative. Radiant energy will be produced when the coal and rock is loaded, and is a considerably lower than deformation energy. Kinetic energy will only be generated when the magnitude and rate of elastic energy release reach a certain level. To simplify the energy evolution of the rock during the uniaxial compression, kinetic and radiant energy were not considered. The plastic and surface energies combined to provide the dissipative energy [38–40].

According to some study of researchers, elastic energy is denoted as follows:

$$U_{sp} = \frac{\sigma_p^2}{2E} \quad (1)$$

where  $\sigma_p$  is stress on the curve,  $U_{sp}$  is elastic energy on the stress-strain curve, and  $E$  is the elastic module. The dissipative energy can be calculated as the area under a stress-strain curve; therefore, the whole energy can be calculated as follows:

$$W_{\Sigma p} = \int_0^{\varepsilon_p} \sigma d\varepsilon \quad (2)$$

$$U = U_{sp} + U_{hp} \quad (3)$$

where  $\sigma$  is the stress of previous point  $p$ ,  $\varepsilon_p$  is the strain of point  $p$ ,  $U_{hp}$  is the dissipative energy on the stress-strain curve, and  $U$  is the total energy on the curve.

##### 2. Energy evolution analysis of yellow sandstone

As can be seen from Equations (1) and (2), The total, elastic, and dissipative energies can be obtained through the stress-strain curve data. To obtain these energies, Origin software (OriginLab Corporation, Northampton, MA, USA) was used, as shown in Figure 11.

According to the law of conservation of energy, only elastic, and dissipative energies exist in the rock system. The elastic energy is primarily used to resist deformation and the dissipative energy is used for the initiation, expansion and development of the cracks in rock and coal, and their combined macroscopic effect is irreversible deformation.

As evident from Figure 11, the growth rate of initial dissipative energy of the yellow sandstone is higher than that of the elastic energy. In the initial deformation stage, the micro-crack closure and friction in the yellow sandstone consumed maximum energy. However, with an increase in deformation, the micro-cracks gradually closed; hence, the effective contact area inside the yellow sandstone increased, and the elastic energy accumulation and dissipative energy growth rates began to decrease. After the elastic curve crossed the dissipative energy curve, the growth rate of elastic energy gradually became more than that of dissipative energy, and the tendency of elastic energy is consistent with that of total energy. Although the dissipative energy curve increased slowly before the peak, it increased sharply after the peak. The total energy of uncoated yellow sandstone and the energy of those coated with 2 mm, 3 mm, 4 mm, and 5 mm of TSL was 0.2637 MJ/m<sup>3</sup>, 0.3255 MJ/m<sup>3</sup>, 0.32023 MJ/m<sup>3</sup>, 0.33706 MJ/m<sup>3</sup>, 0.39105 MJ/m<sup>3</sup>, respectively; the maximal elastic energy was 0.21246 MJ/m<sup>3</sup>, 0.20142 MJ/m<sup>3</sup>, 0.21684 MJ/m<sup>3</sup>, 0.21374 MJ/m<sup>3</sup>, and 0.16322 MJ/m<sup>3</sup>, respectively; the maximal dissipative energy was 0.21402 MJ/m<sup>3</sup>, 0.27522 MJ/m<sup>3</sup>, 0.29147 MJ/m<sup>3</sup>, 0.33623 MJ/m<sup>3</sup>, and 0.35126 MJ/m<sup>3</sup>, respectively. Therefore, it can be deduced that maximal dissipative energy increased with the coating thickness,

and the ductile of TSL impart the confining pressure to specimen and reinforces to the yellow sandstone.

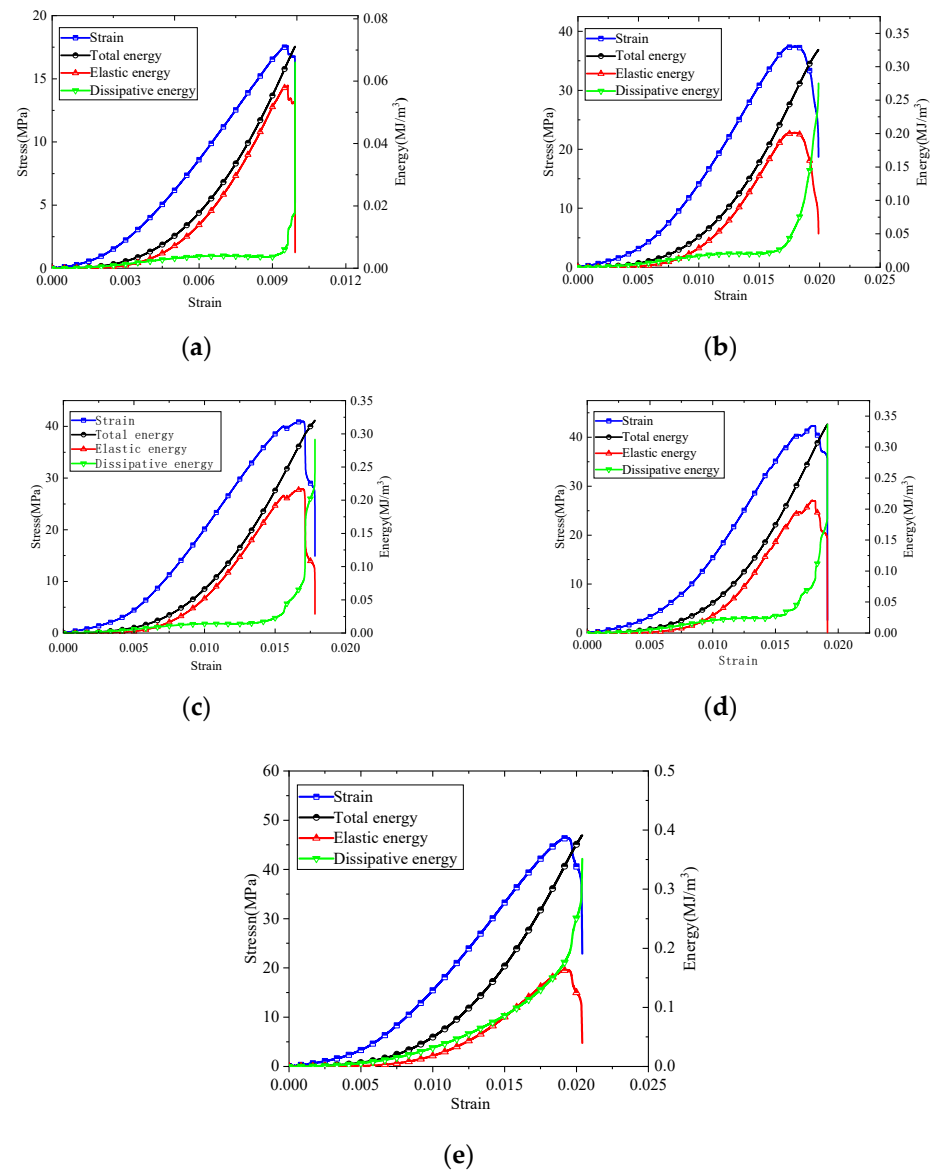


**Figure 11.** Quantitative analysis of energy dynamics of yellow sandstone with different coated thicknesses: (a) TSL coated 0 mm, (b) TSL coated 2 mm, (c) TSL coated 3 mm, (d) TSL coated 4 mm, (e) TSL coated 5 mm.

### 3. Energy evolution analysis of coal

The variation trend of the uncoated coal specimen is the same as that of the uncoated yellow sandstone. The initial dissipative energy of the TSL-coated coal is greater than its elastic energy. Some step-like patterns were observed after the peak of dissipative and elastic energy curves of the TSL-coated coal. Compared with the uncoated coal, the dissipative energy growth rate of TSLs coated coal increases greatly and less sharply after the peak. As evident from Figure 12, the total energy of uncoated coal and those coated with 2 mm, 3 mm, 4 mm of TSL was  $0.07113 \text{ MJ/m}^3$ ,  $0.20807 \text{ MJ/m}^3$ ,  $0.18087 \text{ MJ/m}^3$ , and  $0.21907 \text{ MJ/m}^3$ , respectively; the maximal elastic energy was  $0.05863 \text{ MJ/m}^3$ ,  $0.07708 \text{ MJ/m}^3$ ,  $0.10076 \text{ MJ/m}^3$ , and  $0.12464 \text{ MJ/m}^3$ , respectively; and the maximal dissipative energy was  $0.06604 \text{ MJ/m}^3$ ,  $0.19157 \text{ MJ/m}^3$ ,  $0.15719 \text{ MJ/m}^3$ , and  $0.18942 \text{ MJ/m}^3$ , respectively. Therefore it can be inferred that TSL sprayed with high pressure and penetrated the micro-cracks in coal adhered it together. TSL bonded the coal, which is anisotropic, absorbed some energy, and

reinforced its strength. Furthermore, the strength of coal increased with the thickness of the TSL coating.

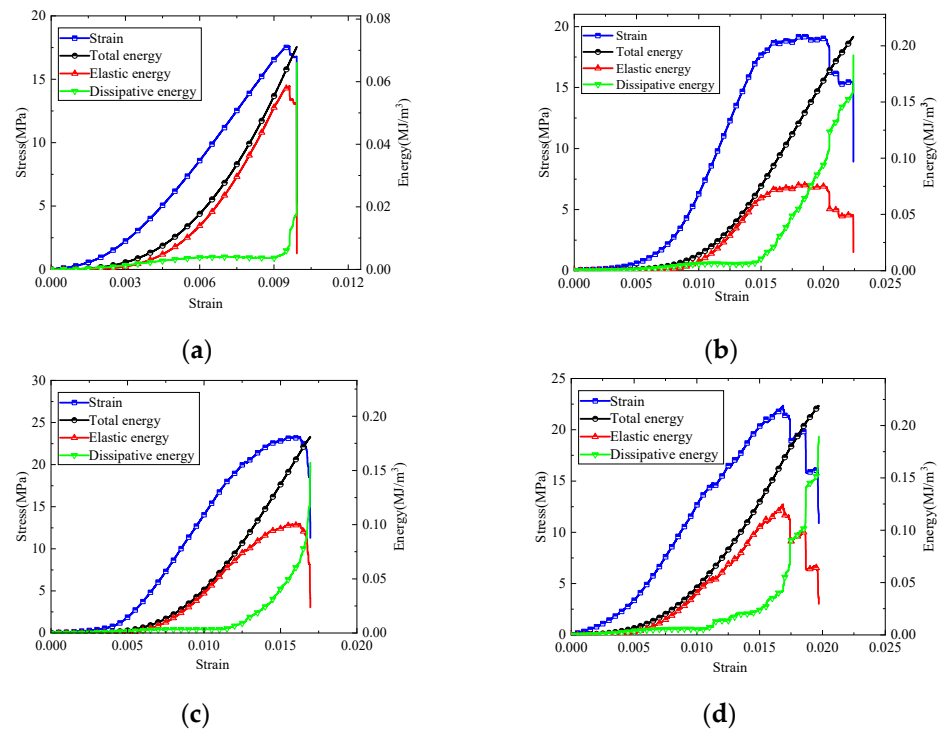


**Figure 12.** Dynamic energy quantitative analysis of coal with different coated thicknesses: (a) TSL coated 0 mm, (b) TSL coated 2 mm, (c) TSL coated 3 mm, (d) TSL coated 4 mm.

#### 4. Energy evolution analysis of white sandstone

The variation trend of coated white sandstone specimen was the same as that of the coated yellow sandstone. There were some step-like patterns after the peak of dissipative and elastic energy curves of the TSL-coated white sandstone. Although the dissipative energy was low before the peak and increased slowly, after the peak, it increased sharply. As can be seen from Figure 13, The total energy of uncoated white sandstone and those coated with 2 mm, 3 mm, 4 mm was 0.29584 MJ/m<sup>3</sup>, 0.33794 MJ/m<sup>3</sup>, 0.33329 MJ/m<sup>3</sup>, and 0.34513 MJ/m<sup>3</sup>, respectively; the elastic energy was 0.23926 MJ/m<sup>3</sup>, 0.19359 MJ/m<sup>3</sup>, 0.21737 MJ/m<sup>3</sup>, and 0.23898 MJ/m<sup>3</sup>, respectively; the dissipative energy was 0.27082 MJ/m<sup>3</sup>, 0.28955 MJ/m<sup>3</sup>, 0.28877 MJ/m<sup>3</sup>, and 0.33785 MJ/m<sup>3</sup>, respectively. Furthermore, the TSL also significantly improved the residual strength of the white sandstone.

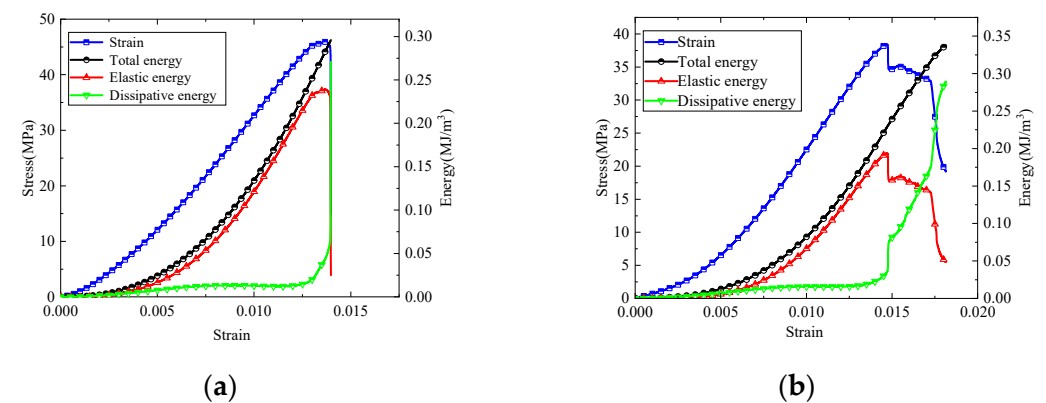


**Figure 13.** Cont.

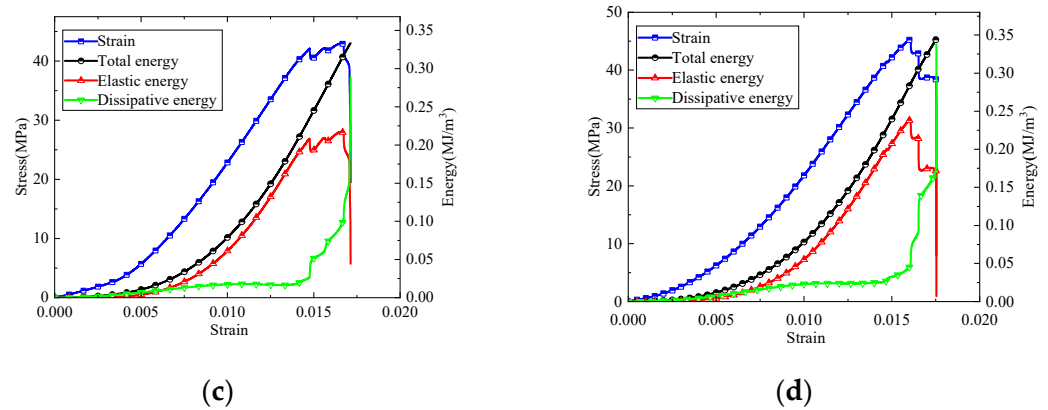


**Figure 13.** Quantitative analysis of energy dynamics of white sandstone with different spray thickness: (a) TSL coated 0 mm, (b) TSL coated 2 mm, (c) TSL coated 3 mm, (d) TSL coated 4 mm.

## 5. Discussion

The UCS improvement of TSL-coated coal over uncoated coal was more significant than that of coated white and yellow sandstone over their respective uncoated counterparts. Coal is anisotropic, and its elastic modulus and uniaxial compressive strength are less than that of the white and yellow sandstones. Sandstones are compacted rocks, and the increment of the UCS in their TSL-coated specimen is small unless the coating thickness is increased. The TSL-coated coal specimen appeared “fat” and swollen in the middle under uniaxial compression load, as shown in the Figure 6. The coal specimen could have been completely destroyed without TSL coating.

TSLs can penetrate the cracks and fissures to reinforce the strength of rocks and coal, the film covering on the surfaces of rock and coal has tensile and shear strength to support them.

With an increment in the coating thickness, the total and dissipative energies of the yellow sandstone specimen increased gradually, the elastic energy was nearly unchanged, and the total energy proportion decreased gradually. The total, dissipative, and elastic energies of coal specimen also increased gradually, and the total energy is approximately 2–3 times more than that of the uncoated coal specimen; thus, the difference was distinct. The total energy of white sandstone increases gradually, and the elastic and dissipative energies were nearly unchanged; the dissipative energy did increase a little but this increase was insignificant.

As evident from Figure 12, the total energy is exerted by the machine on the rock before the peak of the uniaxial compression, which indicates the energy absorbing capability of the rock. For coal specimens, because the total and elastic energies have a positive correlation with the coated thickness, when the total energy is added with the increment in the coating thickness, the energy absorbing capability improves. Elastic energy is energy stored when the rock is deformed, and its magnitude is related to the rock’s characteristics and its elastic deformation. The rock will be destabilized and destroyed when the elastic energy which is stored inside the rock, attains its maximum extent.

With an increment in the coating thickness, the elastic energy in the peak of coal is increased, which indicates that both the energy of storage capacity and the energy-absorbing capacity increased. For the yellow sandstone, with an increment in the coating thickness, the total energy in the peak of yellow sandstone increased gradually but the elastic energy was nearly unchanged; therefore, the energy-absorbing capacity was increased. The total, elastic, and plastic energies of white sandstone were not varied; therefore, the energy-absorbing capacity was nearly constant. The energy-absorbing capacity of coal gradually decreased, and its strength reduced.

TSLs can improve the strength and total energy capacity of coal and rocks through different coating thickness, which can maintain and reinforce the stability of the coal and rocks.

The suitable coating thickness is approximately 2–3 mm considering its cost and operation time. The TSLs' performance can be adjusted based on the on-site different requirement.

## 6. Conclusions

In this paper, TSLs were prepared by controlling the mixing ratio of slurry with high precision, and uniaxial compression experiments were performed on the different thickness combinations of TSL coating on coal and rocks. The improvement in the mechanical properties of the TSL-coated rock specimens and the evolution law of elastic and dissipation energy during the failure process of the sample were analyzed. The following conclusions can be drawn from the study:

- (1) The hard and soft segments of TSLs cause microphase separation and form the physical cross-linking, as seen in their microscopic images. The hard segment was dispersed evenly in the soft segment, which improved the mechanical strength of the TSL.
- (2) The UCS improved with an increased thickness of TSL coating on coal, yellow sandstone, and white sandstone, and the improvements were more obvious because UCS was minimal. The UCS increment was 4.6%, 25.51%, and 43.75% in white sandstone, yellow sandstone, and coal, respectively. The confining pressure was affected by the TSL-coated coal and rocks, which improved the mechanical strength of the rocks and coal under UCS loading.
- (3) Compared with the uncoated coal, the maximal stress resistance of coal coated with 2 mm, 3 mm, and 4 mm of TSLs improved 34.56%, 43.75%, and 34.75%, respectively. The post-peak pressure curves of TSL-coated coal and rocks were more gradual than that of their uncoated counterpart, and they had a step-like pattern, which indicated that the TSL significantly improved the residual strength of the coal and rocks, and increased the reinforcement effect of the confining pressure exerted by the TSL on the coal specimen. The reinforcement of TSLs will be weakened if they are debonded or delaminated from the coal and rock.
- (4) With an increment in the coating thickness, the maximal total, and dissipative energies of yellow sandstone specimen were gradually increased, and the maximal elastic energy was nearly unchanged; The maximal total, elastic, and dissipative energies of TSL-coated coal increased 2–3 times than that of uncoated coal; thus, the increment in coated coal was significant. For the white sandstone, the maximal elastic energy was nearly unchanged, and the maximal total and dissipative energies increased. The energy-absorbing capacity of the coated rocks gradually reduced as the rock strength decreased, and it was higher in coal than that in the yellow and white sandstone. Because coal is an anisotropic material, its total energy is weaker than that of yellow and white sandstones. The TSL reinforcement was significantly more effective for coal.

**Author Contributions:** Conceptualization, Y.Z.; methodology, Y.S.; formal analysis, X.F. (Xiang Fu); investigation, Y.S. and B.Z.; writing—original draft preparation, X.F. (Xiang Fu); writing—review and editing, X.F. (Xiang Fu), X.Z. and Y.C.; visualization, X.F. (Xingyu Fu); supervision, Y.Z.; project administration, Y.Z. and X.F. (Xiang Fu); funding acquisition, Y.Z., X.Z. and Y.C. All authors have read and agreed to the published version of the manuscript.

**Funding:** This research was funded by Major Scientific and Technological Innovation Project in Shandong Province under grant No. 2019SDZY01 and 2019SDZY02, and Yue Qi Distinguished Scholar Project of China University of Mining & Technology (Beijing) under grant No. 2017JCB02.

**Institutional Review Board Statement:** Not applicable.

**Informed Consent Statement:** Not applicable.

**Data Availability Statement:** Data sharing not applicable.

**Acknowledgments:** The authors fully acknowledged Major Scientific and Technological Innovation Project in Shandong Province grant No. 2019SDZY01 and 2019SDZY02, and Yue Qi Distinguished

Scholar Project of China University of Mining & Technology (Beijing) grant No. 2017JCB02. The authors gratefully acknowledge the help and comments of reviewers and editors.

**Conflicts of Interest:** The authors declare no conflict of interest.

## References

1. He, M.C.; Xie, H.P.; Peng, S.P.; Jiang, Y.D. Study on rock mechanics in deep mining engineering. *Chin. J. Rock Mech. Eng.* **2005**, *24*, 2803–2813.
2. Xu, Z.M.; Huang, R.Q. Relationship between rock burst and blasting. *Chin. J. Rock Mech. Eng.* **2003**, *22*, 414–419.
3. Zhang, N.; Han, C.L.; Xie, Z.Z. Theory of continuous beam control and high efficiency supporting technology in coal roadway. *J. Min. Strat. Control Eng.* **2019**, *1*, 1–8.
4. Chen, Y.G.; Lu, S.L. *Coal Mining Ground Control of China*; China University of Mining and Technology Press: Xuzhou, China, 1994.
5. Robertson, S.B.; Molinda, G.M.; Dolinar, D.R.; Pappas, D.M. Best Practices and Bolting Machine Innovations for Roof Screening. Available online: <https://www.cdc.gov/niosh/mining/UserFiles/works/pdfs/bpabm.pdf> (accessed on 3 March 2019).
6. Ozturk, H.; Guner, D. Failure analysis of thin spray-on liner coated rock cores. *Eng. Fail. Anal.* **2017**, *79*, 7925–7933. [[CrossRef](#)]
7. Stacey, T.R. Review of membrane support mechanisms, loading mechanisms, desired membrane performance, and appropriate test methods. *J. South. Afr. Inst. Min. Metall.* **2001**, *101*, 343–351.
8. Kanda, M.J.; Stacey, T.R. Review of the practical effectiveness of thin spray-on liners based on information from suppliers and observations from the mining industry. In *MGR 2019, Proceedings of the First International Conference on Mining Geomechanical Risk, Perth, Australia, 9–11 April 2019*; Australian Centre for Geomechanics: Perth, Australia, 2019; pp. 443–458. [[CrossRef](#)]
9. Manson, D.P.; Stacey, J.R. Support to rock excavations provided by sprayed liners. *Int. J. Rock Mech. Min. Sci.* **2008**, *45*, 773–788. [[CrossRef](#)]
10. Yilmaz, H. Shear-bond strength testing of thin spray-on liners. *J. South. Afr. Inst. Min. Metall.* **2007**, *107*, 519–530.
11. Archibald, J.F.; DeGagné, D.O. Spray-on lining support in Canadian underground mining—a research summary. *CIM Bull.* **2001**, *94*, 49–56.
12. Shan, Z.J.; Porter, I.; Nemcik, J.; Zhang, Z.Y. Investigation on the Rock Surface Support Performance of Welded Steel Mesh and Thin Spray-On Liners Using Full-Scale Laboratory Testing. *Rock Mech. Rock Eng.* **2020**, *53*, 171–183. [[CrossRef](#)]
13. Lau, V.; Saydam, S.; Cai, Y.; Mitra, R. Laboratory Investigation of Support Mechanism for Thin Spray-on Liners. In *Proceedings of the 12th International Conference of International Association for Computer Methods and Advances in Geomechanics, Goa, India, 1–6 October 2008*; pp. 1381–1388.
14. Shi, L. Development of study on support mechanism of sprayed concrete liners in tunneling and caving engineering. *Chin. J. Undergr. Space Eng.* **2011**, *7*, 759–763.
15. Tannant, D.D. Thin spray-on liners for underground rock support. In *Proceedings of the 17th International Mining Congress and Exhibition of Turkey—IMCET, Ankara, Turkey, 19–22 June 2001*; pp. 57–73.
16. Almusallam, A.A.; Khan, F.M.; Dulaijian, S.U.; Al-Amoudi, O.S.B. Effectiveness of surface coatings in improving concrete durability. *Cem. Concr. Compos.* **2003**, *25*, 473–481. [[CrossRef](#)]
17. Archibald, J.F.; Lausch, P. Thin spray-on linings for rock failure stabilization. In *Proceedings of the Vail Rocks 1999, The 37th US Symposium on Rock Mechanics (USRMS), Vail, CO, USA, 7–9 June 1999*.
18. Espley, S.; Langille, C.; McCreath, D.R. Innovative liner support trials in underground hardrock mines. *CIM Bull.* **1995**, *88*, 66–74.
19. Ozturk, H.; Guner, D. Laboratory and distinct element analysis of the deformability behaviour of thin spray-on liners. *Int. J. Rock Mech. Min. Sci.* **2019**, *123*, 1–10. [[CrossRef](#)]
20. Ozturk, H. Work of adhesion of thin spray-on liners. *Rock Mech. Rock Eng.* **2012**, *45*, 1095–1102. [[CrossRef](#)]
21. Ozturk, H. Fracture mechanics interpretation of thin spray-on liner adhesion tests. *Int. J. Adhes. Adhes.* **2012**, *34*, 17–23. [[CrossRef](#)]
22. Ozturk, H.; Tannant, D.D. Thin spray-on liner adhesive strength test method and effect of liner thickness on adhesion. *Int. J. Rock Mech. Min. Sci.* **2010**, *47*, 808–815. [[CrossRef](#)]
23. Yilmaz, H. *Development of Testing Methods for Comparative Assessment of Thin Spray-On Liner Shear and Tensile Properties*; University of the Witwatersrand: Johannesburg, South Africa, 2011.
24. Stacey, T.; Yu, X. Investigations into mechanisms of rock support provided by sprayed liners. In *Ground Support in Mining and Underground Construction, Proceedings of the Fifth International Symposium on Ground Support, Perth, Australia, 28–30 September 2004*; Villaescusa, E., Potvin, Y., Eds.; Taylor and Francis Group: London, UK, 2004; pp. 565–569.
25. Goodman, R.E. *Introduction to Rock Mechanics*; Wiley Press: Toronto, ON, Canada, 1980.
26. Li, Z.C.; Tenney, J.; Chalmers, D.; Mitra, R.; Saydam, S. Application of thin spray on liners to enhance the pre-drained coal seam gas quality. *Energy Explor. Exploit.* **2016**, *34*, 746–765. [[CrossRef](#)]
27. Li, Z.C.; Saydam, S.; Mitra, R.; Chalmers, D. Potential use of thin spray-on liners for gas management in underground coal mines. *J. South. Afr. Inst. Min. Metall.* **2016**, *116*, 1091–1100. [[CrossRef](#)]
28. Hussain, F.; Saydam, S.; Mitra, R.; Cinar, Y. Experimental study for reducing gas inflow by use of thin spray-on liners in underground coal mines. *Min. Technol.* **2012**, *121*, 61–67. [[CrossRef](#)]
29. Li, Z.C.; Hussain, F.; Mitra, R.; Saydam, S. Effectiveness of thin spray-on liners as a gas management tool in underground coal mines. *Int. J. Coal Geol.* **2016**, *168*, 193–201. [[CrossRef](#)]

30. ASTM-638; Standard Test Method for Tensile Properties of Plastic. ASTM: West Conshohocken, PA, USA, 2012. Available online: <https://www.astm.org/d0638-03.html?msclid=65946ecaced411ecbd0f70fe066c6785> (accessed on 15 May 2019).
31. Rinaldi, R.G.; Boyce, M.C.; Weigand, S.J.; Londono, D.J.; Guise, M.W. Microstructure evolution during tensile loading histories of a polyurea. *J. Polym. Sci. Part B Polym. Phys.* **2011**, *49*, 1660–1671. [[CrossRef](#)]
32. Iqbal, N.; Tripathi, M.; Parthasarathy, S.; Kumar, D.; Roy, P.K. Polyurea coating for enhanced blast-mitigation: A review. *R. Soc. Chem. Adv.* **2016**, *6*, 109706–109717. [[CrossRef](#)]
33. Gong, S.Y.; Dou, L.M.; Xu, X.J.; He, J. Experimental study on the correlation between stress and P-wave velocity for burst tendency coal-rock samples. *J. Min. Saf. Eng.* **2012**, *29*, 67–71.
34. Zeng, H.; Lv, Y.Z.; Tang, X.M.; Zou, G.G. Relationship between P-wave & S-wave and density of coal and rock in Sihe mining area. *Coal Technol.* **2017**, *36*, 101–103.
35. Liu, B.; Zhao, Y.X.; Zhang, C.; Zhou, J.L.; Li, Y.T.; Sun, Z. Characteristic strength and acoustic emission properties of weakly cemented sandstone at different depths under uniaxial compression. *Int. J. Coal Sci. Technol.* **2021**, *8*, 1351–1370. [[CrossRef](#)]
36. Guo, Y.X.; Zhao, Y.H.; Wang, S.W.; Feng, G.R.; Zhang, Y.J.; Ran, H.Y. Stress-strain-acoustic responses in failure process of coal rock with different height to diameter ratios under uniaxial compression. *J. Cent. South Univ.* **2021**, *28*, 1724–1736. [[CrossRef](#)]
37. Hou, Y.L.; Lv, X.Y.; Zheng, G.; Huo, J.F. Stress-strain relationship of recycled aggregate concrete under uniaxial compression. *Bull. Chin. Ceram. Soc.* **2015**, *34*, 3102–3105.
38. Zhang, Z.Z.; Gao, F. Experimental research on energy evolution of red sandstone samples under uniaxial compression. *Chin. J. Rock Mech. Eng.* **2012**, *31*, 953–962. [[CrossRef](#)]
39. Zhang, Z.Z.; Gao, F. Experimental investigations on energy evolution characteristics of coal, sandstone and granite during loading process. *J. Chin. Univ. Min. Technol.* **2015**, *44*, 416–422.
40. Liu, J.W.; Huang, B.X.; Wei, M.T. Influence of cyclic uniaxial loading on coal elastic-plastic properties and energy accumulation and dissipation. *J. Liaoning Tech. Univ.* **2012**, *31*, 26–30.